Validation of the gFR Computational Fluid Dynamics Methodology

Daniel Eager[1], Kurt Aikens[2]
Physics Dept., Houghton College, 1 Willard Ave, Houghton, NY 14744
[1]daniel.eager18@houghton.edu, [2]kurt.aikens@houghton.edu

Abstract

There is a current demand in computational fluid dynamics (CFD) for higher-order solvers that can simulate fluid flows using unstructured grids. Such software would allow for highly-accurate simulations of complex and industrially-relevant geometries. To help meet these needs, a new code, gFR, is being developed by researchers at the NASA Glenn Research Center. It is based on the flux reconstruction (FR) methods of H.T. Huynh, which are used to solve the three-dimensional Navier-Stokes equations. The methodology is capable of performing efficient and accurate large eddy simulations (LES) and, depending on user-specified choices, can recover many popular high-order methods including the discontinuous Galerkin, spectral difference, and spectral volume methods. Runge-Kutta methods are used to advance the governing equations in time. While gFR has many theoretical advantages, it had only been tested on two problems prior to the present work: a two-dimensional inviscid vortex and the Taylor-Green vortex problem. The present study at Houghton College includes tests of laminar flow over a flat plate as well as laminar channel flow over a backward-facing step. Preliminary results are shown for the two test cases and compared with corresponding experimental and theoretical results. Challenges are described and possible future work is outlined.

gFR Methodology

The gFR code [1,2] uses the flux reconstruction method [3] to discretize the advection terms (e.g., $\partial F/\partial x$) in the Navier-Stokes equations. In this method, the domain is discretized and each cell is further subdivided into solution and flux points. This is illustrated in Figure 1 for two cells, *j* and *j*+1. For *P*+1 flux points, an interpolating polynomial of degree *P* is fit to the flux values at each. However, the polynomial, $f^D(x)$, is often discontinuous across cell interfaces. To correct this, a new flux function, $F(x)$, is generated in each cell and constrained to be continuous at cell boundaries. This is accomplished by adding a *P*+1-order correction function to $f^D(x)$. It is chosen to approximate zero over much of the cell but to enforce the common upwind flux, f^*, at cell boundaries. Many popular finite-element methodologies are recovered depending on the choice of this correction function. Finally, $\partial F/\partial x$ is estimated using the derivative of $F(x)$, and the formal order of accuracy can be increased by increasing *P*. This overall approach has been extended to three dimensions in the gFR code and a similar process is used for estimating diffusion terms in the governing equations.

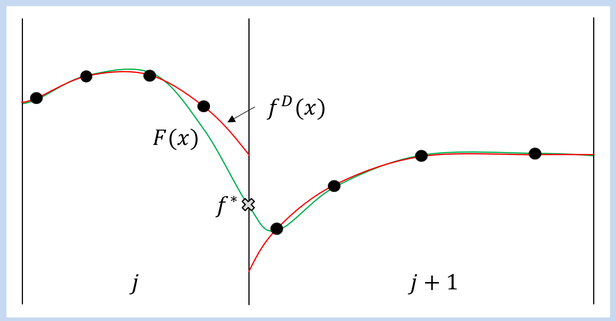

Figure 1. A depiction of polynomial interpolation in the gFR code, showing the discontinuous and continuous fluxes within two cells, j and j+1.

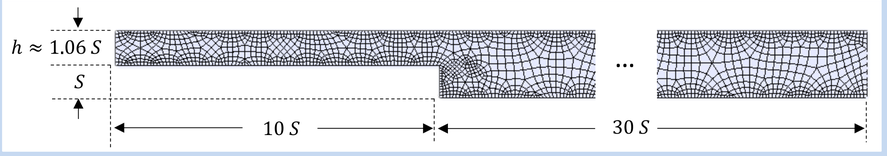

Figure 2. The geometry used for simulations of laminar channel flow over a backward-facing step. S is the height of the step and h is the upstream channel height. The flow is from left to right. The unstructured grid shown has approximately a third of the number of cells as the grid that is used here.

Simulation Details

Test cases are completed for approximately incompressible (i.e., a freestream Mach number of 0.1) laminar flow over a flat plate as well as laminar channel flow over a backward-facing step. The correction function that recovers the discontinuous Galerkin method is utilized here with the Gauss points for solution and flux points. The third-order SSP Runge-Kutta method is used for integrating in time with locally-determined timesteps (CFL=0.1) to accelerate convergence. Both simulations use a uniform-velocity subsonic inflow and a subsonic outflow boundary condition.

The flat plate simulations are performed for a Reynolds number of 10^4 (based on plate length) and the plate is assumed to be isothermal. This boundary condition was found to be more stable than an adiabatic boundary condition. Multiple grids are used, closely modeled after grids from the International Workshop on High-Order Methods (HOW, for "high-order workshop"). These cases include a fluid region upstream of the start of the plate. A separate series of simulations are performed where the plate begins at the inflow boundary.

The laminar flow over a backward-facing step was modeled after the experimental set up of Armaly, et al. [4], shown from the side in Figure 2. Isothermal walls are specified at the top and bottom of the geometry. Two-dimensional simulations are performed at a series of Reynolds numbers (based on twice the upstream channel height, $2h$) from 100 to 1000. The utilized grid has 9700 cells that are preferentially clustered near the walls and the step.

Acknowledgements

We would like to thank the Houghton College Summer Research Institute for funding and XSEDE for access to TACC Stampede. Furthermore, we are grateful for the support of our collaborators H.T. Huynh, Jim DeBonis, and Seth Spiegel. H.T. developed the flux reconstruction methods and put us in touch with Jim, Jim formulated the project, and Seth supported our using gFR. We are also thankful to Seth for his work in developing the code. While we did run in to some problems, we found the code to be very usable with a small learning curve.

References

[1] S. C. Spiegel, H. T. Huynh and J. R. DeBonis, "A survey of the isentropic Euler vortex problem using high-order methods," in 22nd AIAA Computational Fluid Dynamics Conference, AIAA Paper No. 2015-244, Dallas, TX, 2015.
[2] S. C. Spiegel, H. T. Huynh and J. R. DeBonis, "De-aliasing through over-integration applied to the flux reconstruction and discontinuous Galerkin methods," in 22nd AIAA Computational Fluid Dynamics Conference, AIAA Paper No. 2015-2744, Dallas, TX, 2015.
[3] H. T. Huynh, "A flux reconstruction approach to high-order schemes including discontinuous Galerkin methods," in 18th AIAA Computational Fluid Dynamics Conference, AIAA Paper No. 2007-4079, Miami, FL, 2007.
[4] B. F. Armaly, F. Durst, J. C. F. Pereira and B. Schonung, "Experimental and theoretical investigation of backward-facing step flow," *J. Fluid Mech,* Vol. 127, pp. 473-496, 1983.
[5] T. P. Chiang and T. W. H. Sheu, "A numerical revisit of backward-facing step flow problem," *Physics of Fluids,* Vol. 11, No. 4, pp. 862-874, 1999.
[6] P. T. Williams and A. J. Baker, "Numerical simulations of laminar flow over a 3D backward-facing step," *International Journal for Numerical Methods in Fluids,* Vol. 24, pp. 1159-1183, 1997.

Results

For both test cases, many more simulations were planned than were found to be possible. Only the lowest-accuracy cases with the coarsest grids converged. That said, the simulation results obtained can still be analyzed.

In the flat-plate simulations using the full-sized HOW grids, unphysical solutions are found near the front of the plate as shown in Figure 3. Upstream of the front of the plate ($x/L = 0$), the fluid is moving faster near the slip wall at the bottom of the image than in the freestream. This artifact also affects the boundary layer as the fluid continues downstream. This is the motivation for shortened grids – to avoid the slip wall/isothermal wall interface. Despite this change, the shortened grids still produce fluid flows that have a velocity overshoot in the boundary layer, as shown in Figure 4. This may be related to the boundary condition formulations and their interaction at the inflow/wall interface.

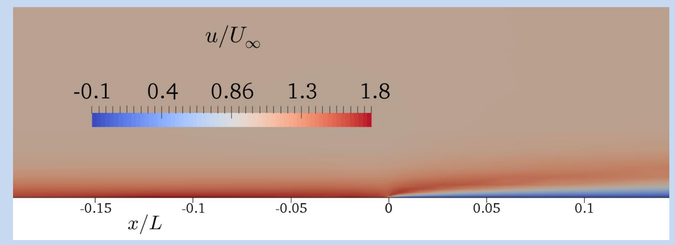

Figure 3. This figure shows contours of the axial velocity, u, normalized by the freestream velocity, U_∞. x/L is the position in the axial direction, non-dimensionalized by the length of the plate – the plate begins at x/L = 0. This representative case uses P = 2 and the coarsest grid tested.

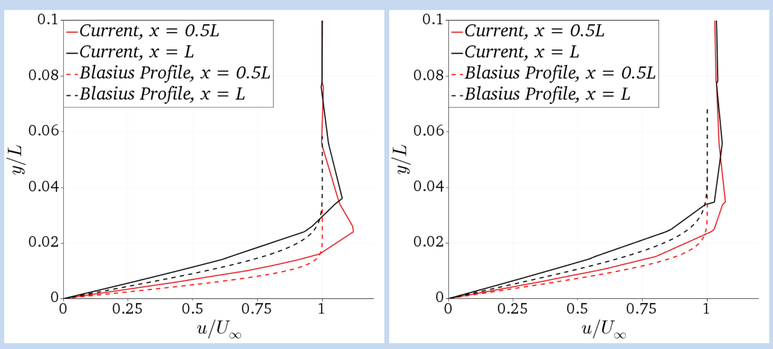

Figure 4. Velocity profiles for the full-sized (left) and shortened (right) grid cases. Profiles are shown at half the plate length and the full plate length. These are compared to the Blasius theory at the same position. The plots are shown with velocity on the x-axis and height above the wall on the y-axis.

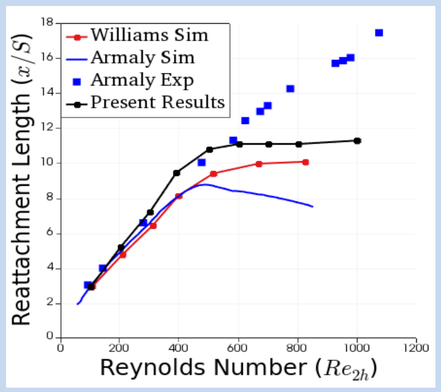

Figure 5. Reattachment length (non-dimensionalized by S) plotted versus the Reynolds number (based on twice the channel height).

The results for simulations of the backward-facing step are shown next and are more promising. Figure 5 shows the reattachment length as a function of Reynolds number. Simulation results are compared with experimental and simulation results from Armaly et al. [4] and simulation data from Williams and Baker [6]. The reattachment length is defined as the distance between the step and the location where the partial derivative of the streamwise momentum with respect to the wall-normal direction is zero, at the wall. This location is estimated using linear interpolation between solution points. All of the simulation results show similar trends to those of the Armaly, et al. experiment until a Reynolds number of about 500. At this point, the experimental flowfield differs from the two-dimensional simulations. This is due to the limited spanwise extent of the experiment. However, the present results show qualitative agreement with those of the other simulations, with the reattachment length leveling off. Next, the velocity profiles at various streamwise locations are compared to the experiment from Armaly, et al. [4] and the simulation results from Chiang and Sheu [5]. These are shown in Figure 6 for a Reynolds number of 100. The gFR results are comparable to the other results and match those of Chiang and Sheu well through Re = 800.

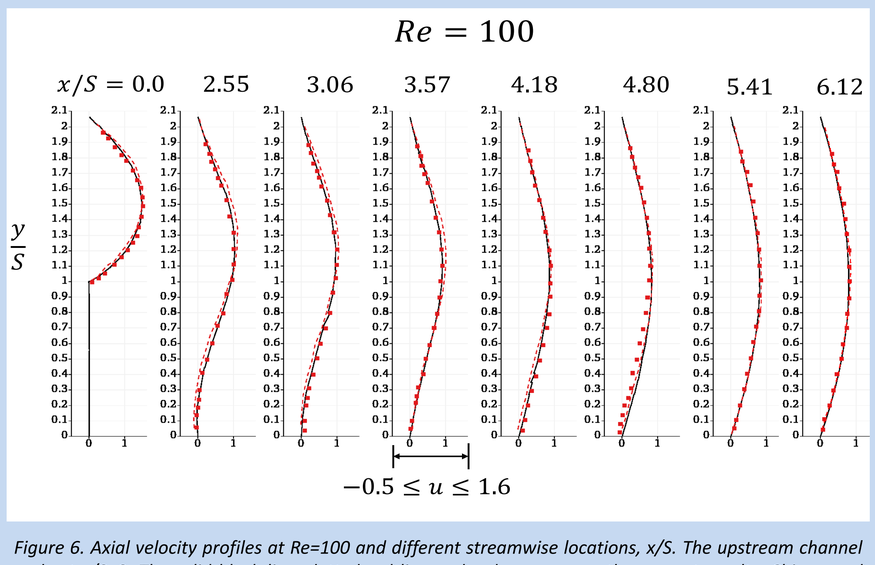

Figure 6. Axial velocity profiles at Re=100 and different streamwise locations, x/S. The upstream channel ends at x/S=0. The solid black line, dotted red line and red squares are the present results, Chiang and Sheu data [5], and Armaly, et al. experimental data [4], respectively.

Conclusions

Overall, the present results show that the gFR code is promising. However, much development work on the boundary conditions and the local time-stepping algorithms remains to be done. Both appear to be limiting the accuracy and grid resolution that can be utilized currently. This makes it difficult to make quantitative comparisons between simulation results and those in the literature. It is also expected that boundary conditions contributed to the unphysical velocity overshoot noted in the flat plate results.

Qualitatively, the data gathered for the backward-facing step simulations are in good agreement with other results and show promise for the future use of the gFR code. The predicted velocity profiles and reattachment lengths compared well with those in the literature for lower Reynolds numbers. For higher Reynolds numbers, the present simulations produced larger reattachment lengths than similar two-dimensional simulations, but comparable trends were noted.

In the future, once better boundary conditions are implemented, testing should include higher orders of accuracy and finer grids for both cases considered here. Furthermore, three-dimensional simulations of the backward-facing step from Armaly, et al. would provide additional validation of the full gFR implementation.